Electrostatics of Ligand Binding: Parametrization of the Generalized Born Model and Comparison with the Poisson−Boltzmann Approach

Hao-Yang Liu and Xiaoqin Zou*

Dalton Cardiovascular Research Center and Department of Biochemistry, University of Missouri, Columbia, Missouri 65211

Received: January 17, 2006; In Final Form: March 1, 2006

An accurate and fast evaluation of the electrostatics in ligand−protein interactions is crucial for computer-aided drug design. The pairwise generalized Born (GB) model, a fast analytical method originally developed for studying the solvation of organic molecules, has been widely applied to macromolecular systems, including ligand−protein complexes. However, this model involves several empirical scaling parameters, which have been optimized for the solvation of organic molecules, peptides, and nucleic acids but not for energetics of ligand binding. Studies have shown that a good solvation energy does not guarantee a correct model of solvent-mediated interactions. Thus, in this study, we have used the Poisson−Boltzmann (PB) approach as a reference to optimize the GB model for studies of ligand−protein interactions. Specifically, we have employed the pairwise descreening approximation proposed by Hawkins et al.[1] for GB calculations and DelPhi for PB calculations. The AMBER all-atom force field parameters have been used in this work. Seventeen protein−ligand complexes have been used as a training database, and a set of atomic descreening parameters has been selected with which the pairwise GB model and the PB model yield comparable results on atomic Born radii, the electrostatic component of free energies of ligand binding, and desolvation energies of the ligands and proteins. The energetics of the 15 test complexes calculated with the GB model using this set of parameters also agrees well with the energetics calculated with the PB method. This is the first time that the GB model has been parametrized and thoroughly compared with the PB model for the electrostatics of ligand binding.

1. Introduction

Most chemical processes take place in solution. It is therefore essential to account for the solvent effect, among which free energies of solvation and the solvation component of free energies of ligand binding are very challenging to calculate.[2] Water molecules affect solvation in two aspects: they substantially screen the electrostatic interactions and result in hydrophobic interactions. A straightforward way to account for the solvent effect is the explicit treatment of water molecules in the molecular dynamics (MD) or Monte Carlo (MC) simulations.[3,4] However, such simulations are computationally expensive and thus not applicable to large database screening for drug design.

Alternatively, continuum solvent models are computationally tractable and reasonably accurate.[5−7] In these continuum models, a solute is treated as charged atoms inside a low dielectric volume (i.e., the volume of the solute) surrounded by a high dielectric medium (e.g., water). Two types of continuum approaches are commonly used, the Poisson−Boltzmann (PB) approaches[8−11] and the generalized Born (GB) approaches.[12,13] The GB model is a simplified model that attempts to capture the physics of the PB equation. The GB approaches have given promising results on calculating solvation energies, free energies of ligand binding, pK_a, and redox properties (see ref 7 for a review). Various GB models have been implemented as effective force fields and are available in CHARMM,[14] AMBER,[15] IMPACT,[16] GROMOS,[17] TINKER,[18] MCPRO,[19] and other molecular modeling software packages. Different versions of the GB model have also been implemented in ligand docking programs, for example, grid-based GB[20] for DOCK4.0,[21] analytical pairwise GB[22] for DOCK5.0,[23] grid-based GB for SEED-FFLD,[24−26] analytical volume GB (AVGB) for MPSim-Dock,[27] and surface GB (SGB)[28] for PLOP[29] combined with either DOCK3.5.54[30] or Glide.[31]

Most GB models involve parametrization of certain scaling factors, which is usually based on the capacity of reproducing either total or the electrostatic component of solvation free energies of a diverse set of molecules.[1,32−38] However, Jayaram et al.[39] found that although the three different versions of the GB formula that were used yield almost identical total solvation energies, the individual energy terms (self and cross) have quite different results. On the basis of the discovery, they argued that an accurate estimate of total solvation energies alone does not necessarily validate an electrostatic model for solvent-mediated interactions. Scarsi and Caflisch[40] showed that even a crude energy model can correctly predict the change in intermolecular electrostatic energy upon solvation of the complex; however, the same model totally mispredicts the intermolecular electrostatic energy in solution. Scarsi et al.[41] also showed that many ligand−protein complexes exhibit a strong anticorrelation between their solvation energies and vacuum energies. In these cases, the total solvation energy is dominant by the gas-phase Coulombic energy and only marginally determined by the energy in solution. The authors therefore argued that a validation of an electrostatic model based on the solvation energy is not sufficient for ligand binding studies. These observations are further supported by the findings of Rankin et al.[42] that a broad range of parameter sets that are optimal for solvation energy

* Corresponding author. E-mail: zoux@missouri.edu. Phone: 573-882-6045. Fax: 573-884-4232.

10.1021/jp060334w CCC: $33.50
Published on Web 04/18/2006

calculations may still lead to large variations in electrostatic binding energies. Using pK_a shift or experimentally determined total binding free energies to validate the parametrization of an electrostatic model are alternative although difficult approaches.[39,40] In this paper, for the first time, the GB model has been parametrized and thoroughly compared with the PB calculations on the electrostatic component of free energies of binding. Development of a fast and relatively accurate electrostatic model for ligand binding is vitally important for computer-aided drug design.

Several GB models have been proposed in the literature.[1,12,28,43−48] These models use different methods to calculate effective Born radii, a quantitative measure of how deep the atoms are buried in the molecular system. One of the methods is the fast, widely used method proposed by Hawkins, Cramer, and Truhlar (denoted as the HCT method),[1] which employs the pairwise descreening approximation for rapid calculations of Born radii and is utilized in the present work.

This paper is organized as follows. In the Method section, we give a brief overview of the GB model and the pairwise descreening approximation for calculations of effective Born radii. We also describe how to calculate the electrostatic component of free energies of ligand binding with the GB and PB methods and how to parametrize the descreening parameters in the HCT version of the GB model. We then present our findings in the Results section. We conclude with a summary and discussion of our results.

2. Method

2.1. Calculation of Effective Born Radii. We first review the calculation of effective Born radii by starting with the Born formula. Consider an ion of radius a and charge q at the center. The electrostatic component of the solvation free energy is then given by[49]

$$\Delta G_{\text{Born}} = G^{\text{solvent}} - G^{\text{vacuum}} = -\frac{q^2}{2a}\left(1 - \frac{1}{\epsilon_w}\right) \qquad (1)$$

where ϵ_w is the dielectric constant of water (80).

In a multiatomic molecule, atom i is represented as a sphere of radius a_i with a point charge q_i at its center. The molecule has a low interior dielectric constant of ϵ_p and is placed in an exterior environment with a dielectric constant of ϵ_{ex}. For arbitrarily shaped molecules, the generalized Born (GB) model[12] is introduced to calculate the electrostatic solvation energy (also referred to as the polarization energy), the difference of the electrostatic energy to transfer a molecule from a *homogeneous* environment ($\epsilon_{ex} = \epsilon_p$) to an aqueous environment ($\epsilon_{ex} = \epsilon_w$). By ignoring the reaction field (i.e., the Coulomb field approximation),[13] the polarization energy of atom i is given by

$$G_{\text{pol},i} = -\frac{q_i^2}{2\alpha_i}\left(\frac{1}{\epsilon_p} - \frac{1}{\epsilon_w}\right) \qquad (2)$$

where α_i is the effective Born radius of atom i.

The GB model approximates the polarization energy of the molecule as[36,41,50]

$$G_{\text{pol}} = -\frac{1}{2}\left(\frac{1}{\epsilon_p} - \frac{1}{\epsilon_w}\right)\sum_i^N\sum_j^N \frac{q_i q_j}{f_{\text{GB}}(r_{ij})} \qquad (3)$$

where r_{ij} is the interatomic distance and $f_{\text{GB}}(r_{ij})$ is a function conventionally written as[12]

$$f_{\text{GB}}(r_{ij}) = \sqrt{r_{ij}^2 + \alpha_i\alpha_j \exp[-r_{ij}^2/(4\alpha_i\alpha_j)]} \qquad (4)$$

The function $f_{\text{GB}}(r_{ij})$ approaches r_{ij} as the two atoms are far apart and becomes the effective Born radius of atom i when $i = j$.

The Born radius of atom i, α_i, depends solely on molecular geometric properties and represents how much atom i is buried in the molecule. α_i is calculated by

$$\frac{1}{\alpha_i} = \frac{1}{a_i} - \frac{1}{4\pi}\int_{in, r>a_i} \frac{1}{r^4}\,dV \qquad (5)$$

Again, a_i is the radius of atom i, or, more exactly, the effective Born radius of isolated atom i.

Calculating the integral in eq 5 is time-consuming. To dramatically improve the computational speed, several approximate approaches have been proposed to replace the integral with the following pairwise summation:

$$\frac{1}{\alpha_i} = \frac{1}{a_i} - \frac{1}{4\pi}\sum_j \int_j \frac{1}{r^4}\,dV \qquad (6)$$

The HCT GB model[1] is one of these pairwise approaches and is used in the present study. In the HCT GB model, the contribution of the integral over the volume of atom j to the Born radius of atom i is written as

$$\frac{1}{4\pi}\int_j \frac{1}{r^4}\,dV = \mathscr{H}(a_i, S_j a_j, r_{ij}) = \frac{1}{2}\left[\left(\frac{1}{L_{ij}} - \frac{1}{U_{ij}}\right) + \left(\frac{S_j^2 a_j^2}{4r_{ij}} - \frac{r_{ij}}{4}\right)\left(\frac{1}{L_{ij}^2} - \frac{1}{U_{ij}^2}\right) + \frac{1}{2r_{ij}}\ln\frac{L_{ij}}{U_{ij}}\right] \qquad (7)$$

where

$$L_{ij} = \begin{cases} 1 & \text{if } a_i \geq r_{ij} + S_j a_j \\ \max(a_i, r_{ij} - S_j a_j) & \text{if } a_i < r_{ij} + S_j a_j \end{cases} \qquad (8)$$

and

$$U_{ij} = \begin{cases} 1 & \text{if } a_i \geq r_{ij} + S_j a_j \\ r_{ij} + S_j a_j & \text{if } a_i < r_{ij} + S_j a_j \end{cases} \qquad (9)$$

If the atoms around atom i did not overlap each other, eqs 6 and 7 with S_j set to unity would give the exact analytical expression for α_i. However, this is not true in real molecules. To account for atomic overlaps, Hawkins et al.[1] introduced the atom-type-dependent descreening parameters $\{S_x\}$.

2.2. Electrostatics of Ligand Binding. The electrostatic component of energies of ligand binding can be calculated using two different approaches, as illustrated in Figure 1. The first approach decomposes the electrostatic binding energy by using a three-step thermodynamic process (Figure 1a), as described in refs 51 and 22. The process starts from the state that the ligand and the receptor are far apart in aqueous solution (upper left in Figure 1a). The first step is to transfer the ligand and the receptor from water to a homogeneous dielectric medium with $\epsilon_{ex} = \epsilon_p$, respectively (lower left in Figure 1a). The respective energy cost is the opposite of the polarization energy, $-G_{\text{pol,L}}$ for the ligand and $-G_{\text{pol,R}}$ for the receptor. The second step is to combine the ligand and receptor into a complex (lower right in Figure 1a); the energy difference is simply the Coulombic energy in a uniform medium ($\epsilon_{in} = \epsilon_{ex} = \epsilon_p$). The final step is

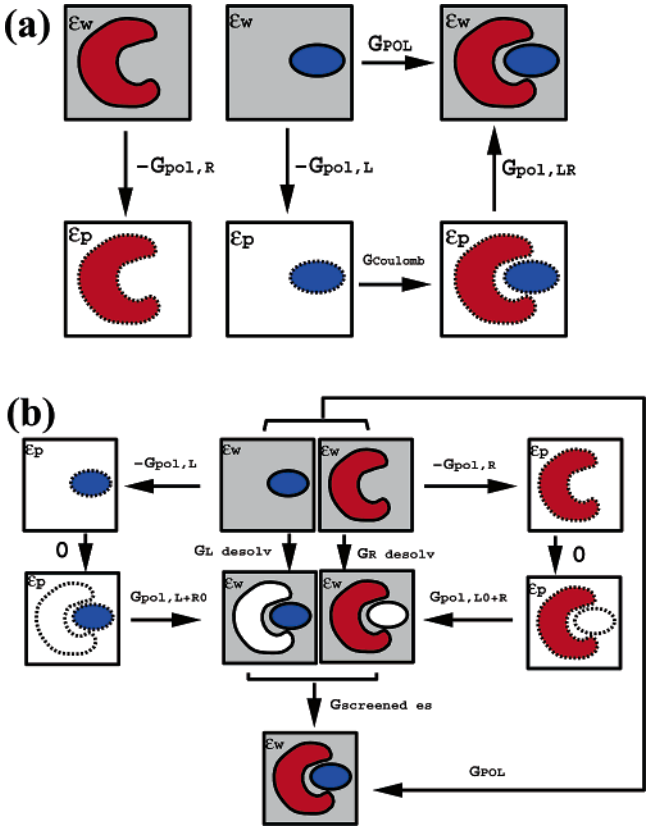

Figure 1. Illustration of two different cycles that were used for decomposition of the electrostatic component of ligand binding energies. The receptor and ligand are colored when they carry atomic charges and plotted in white when their atomic charges are deprived. The surrounding dielectric medium is colored in gray if its dielectric constant is high ($\epsilon_{ex} = \epsilon_w$). A homogeneous dielectric medium is plotted in white ($\epsilon_{ex} = \epsilon_p$), and the boundary of the molecule in this case is plotted in dashed lines to represent essentially no dielectric boundaries.

to solvate the ligand−receptor complex, that is, to transfer the complex from the homogeneous medium to aqueous solution (upper right in Figure 1a). The corresponding energy difference is the polarization energy of the complex, $G_{pol,LR}$. Thus, the electrostatic component of the binding free energy is summed as

$$G_{POL} = G_{pol,LR} - G_{pol,L} - G_{pol,R} + G_{Coulomb} \quad (10)$$

Each term in eq 10 is calculated as

$$G_{pol,L} = -\frac{1}{2}\left(\frac{1}{\epsilon_p} - \frac{1}{\epsilon_w}\right)\sum_i^L\sum_j^L \frac{q_i q_j}{f_{GB}^L(r_{ij})} \quad (11)$$

$$G_{pol,R} = -\frac{1}{2}\left(\frac{1}{\epsilon_p} - \frac{1}{\epsilon_w}\right)\sum_i^R\sum_j^R \frac{q_i q_j}{f_{GB}^R(r_{ij})} \quad (12)$$

$$G_{pol,LR} = -\frac{1}{2}\left(\frac{1}{\epsilon_p} - \frac{1}{\epsilon_w}\right)\sum_i^{L+RL+R}\sum_j \frac{q_i q_j}{f_{GB}^{LR}(r_{ij})} \quad (13)$$

$$G_{Coulomb} = \frac{1}{\epsilon_p}\sum_i^L\sum_j^R \frac{q_i q_j}{r_{ij}} \quad (14)$$

where L, R, and LR represent the ligand alone, the receptor alone, and the ligand−receptor complex, respectively. f_{GB}^L, f_{GB}^R, and f_{GB}^{LR} are calculated in the corresponding environments.

The second approach is illustrated in Figure 1b (see the cycle at the center of the panel). G_{POL} is the sum of $G_{L\ desolv}$, $G_{R\ desolv}$, and $G_{screened\ es}$, where the three terms are the partial desolvation energy of the ligand, partial desolvation energy of the receptor, and screened electrostatic energy, respectively.

$$G_{POL} = G_{L\ desolv} + G_{R\ desolv} + G_{screened\ es} \quad (15)$$

Each term in eq 15 is calculated as[20,22]

$$G_{L\ desolv} = \frac{1}{2}\left(\frac{1}{\epsilon_p} - \frac{1}{\epsilon_w}\right)\sum_i^L\sum_j^L \left[\frac{q_i q_j}{f_{GB}^L(r_{ij})} - \frac{q_i q_j}{f_{GB}^{LR}(r_{ij})}\right] \quad (16)$$

$$G_{R\ desolv} = \frac{1}{2}\left(\frac{1}{\epsilon_p} - \frac{1}{\epsilon_w}\right)\sum_i^R\sum_j^R \left[\frac{q_i q_j}{f_{GB}^R(r_{ij})} - \frac{q_i q_j}{f_{GB}^{LR}(r_{ij})}\right] \quad (17)$$

$$G_{screened\ es} = \frac{1}{\epsilon_p}\sum_i^L\sum_j^R \frac{q_i q_j}{r_{ij}} - \left(\frac{1}{\epsilon_p} - \frac{1}{\epsilon_w}\right)\sum_i^L\sum_j^R \frac{q_i q_j}{f_{GB}^{LR}(r_{ij})} \quad (18)$$

An alternative method to calculate $G_{L\ desolv}$ and $G_{R\ desolv}$, which was used for PB calculations in the present work, is explained as follows. Take the ligand as an example. The thermodynamic cycle for the calculation of $G_{L\ desolv}$ is illustrated in Figure 1b, the left cycle. Specifically, the fully solvated ligand is transferred to a medium with dielectric constant ϵ_p (upper left in Figure 1b), at the energy cost of $-G_{pol,L}$. A molecule that is identical to the receptor except carrying no atomic charges (denoted as R0) is then placed to the position that the receptor locates in the ligand−receptor complex (lower left in Figure 1b). Because the dielectric constant of R0 is ϵ_p, the same as that of the exterior environment, the energy of the system remains the same. Finally, the complex of the ligand and R0 is fully solvated. The corresponding energy difference is the polarization energy of the complex, $G_{pol,L+R0}$. The thermodynamic cycle can be described by the following equation:

$$G_{L\ desolv} = G_{pol,L+R0} - G_{pol,L} \quad (19)$$

It is obvious from eq 3 that

$$G_{pol,L+R0} = -\frac{1}{2}\left(\frac{1}{\epsilon_p} - \frac{1}{\epsilon_w}\right)\sum_i^L\sum_j^L \frac{q_i q_j}{f_{GB}^{LR}(r_{ij})} \quad (20)$$

because every atom of R0 has no charge.

Similarly, based on the thermodynamic cycle illustrated on the right-hand side of Figure 1b, $G_{R\ desolv}$ can be calculated as

$$G_{R\ desolv} = G_{pol,L0+R} - G_{pol,R} \quad (21)$$

Obviously,

$$G_{pol,L0+R} = -\frac{1}{2}\left(\frac{1}{\epsilon_p} - \frac{1}{\epsilon_w}\right)\sum_i^R\sum_j^R \frac{q_i q_j}{f_{GB}^{LR}(r_{ij})} \quad (22)$$

2.3. PB Calculations. All of the PB calculations were carried out using the DelPhi program,[9] with the same vdw radius and charge assignments as those for the GB calculations. The dielectric constant was set to 4 for solute molecules and 80 for the solvent. The grid spacing was set to 0.33 Å (i.e., three grid points per angstrom). The "perfil" parameter, defined as the percentage of the longest linear dimension of the object in study

TABLE 1: Complexes Studied in the Present Work

complex	G_{POL} by PB (kcal/mol)	resl (Å)	protein/ligand
		rraining complexes	
3ptb-benz	−1.58	1.7	trypsin/benzamidine
4dfr-mtx	−4.46	1.7	dihydrofolate reductase/methotrexate
2ifb-PLM	1.70	2.0	fatty acid binding protein/C15COOH
6abp-ara	12.70	1.67	L-arabinose binding protein M108L/L-arabinose
1rnt-2gp	15.88	1.9	ribonuclease T1/2-GMP
1fkf-fk5	3.80	1.7	FK506 binding protein/FK506
1drf-fol	0.80	2.0	dihydrofolate reductase/folate
1hsl-his	−0.18	1.89	histidine binding protein/Histidine
1aaq-psi	18.60	2.5	HIV-1 protease/hydroxyethylene isostere
1ppc-nap	1.93	1.8	trypsin/NAPAP
1tng-amc	−2.64	1.8	trypsin/aminomethylcyclohexane
1pgp-6pg	17.85	2.5	6-PGDH/6-phosphogluconic acid
1pph-tap	1.27	1.9	trypsin/3-TAPAP
7abp-fca	14.47	1.67	l-arabinose binding protein M108L/D-fucose
2gbp-glc	12.04	2.9	galactose binding protein/galactose
1nsd-dan	20.34	1.80	neuraminidase/DANA
1rbp-rtl	5.33	2.00	retinol-binding protein/retinol
		test complexes	
1ajv-nmb	12.65	2.0	HIV-1 protease/AHA006
1a9t-two	34.96	2.0	PNP/9-deazainosine
1dwd-mid	7.36	3.0	thrombin/NAPAP
1ets-pap	11.61	2.3	thrombin/NAPAP
1abe-ara	11.35	1.7	L-arabinose binding protein/L-arabinose
1mdq-mal	19.08	1.9	maltose binding protein A301GS/maltose
1l83-bnz	0.12	1.7	lysozyme/benzene
4ts1-tyr	5.66	2.5	tyrosyl-transfer RNA synthetase/tyrosine
2mcp-PC	−0.12	3.1	immunoglobulin/phosphocholine
1ulb-gun	2.75	2.75	PNP/guanine
3fx2-fmn	26.24	1.9	flavodoxin/FMN
8atc-pal	1.36	2.5	aspartate carbamoyltransferase/PALA
1nnb-dan	19.32	2.80	neuraminidase/DANA
2pk4-aca	−9.47	2.25	plasminogen kringle 4/aminocaproic acid
7tim-pgh	6.12	1.9	trisephosphate isomerase/phosphoglycolohydroxamate

to the linear dimension of the lattice, was set to 90%. The rest of the control parameters were set to the default values in the program.

Notice that the "corrected reaction field energy" term in the output of DelPhi refers to the energy difference for transferring a molecular system from a homogeneous reference environment ($\epsilon_{ex} = \epsilon_p$) to an aqueous environment ($\epsilon_{ex} = \epsilon_w$), that is, G_{pol} in eq 3. Therefore, applying DelPhi to the thermodynamic cycle illustrated in Figure 1a yielded $G_{pol,L}$ (corrected reaction field energy for the ligand alone), $G_{pol,R}$ (for the receptor alone), $G_{pol,LR}$ (for the ligand−receptor complex), and G_{POL} (eq 10). The results were compared with the GB results calculated using eqs 10−13.

Two other energy components, $G_{L\ desolv}$ and $G_{R\ desolv}$, were calculated using eqs 19−22 with DelPhi, as illustrated in Figure 1b. Notice that $G_{pol,L+R0}$ in eq 19 is simply the corrected reaction field energy for the complex of the ligand and R0 and $G_{pol,L0+R}$ in eq 21 is that for the complex of the receptor and L0. The PB results were compared with the GB results calculated using eqs 16 and 17.

2.4. Preparation of the Training and Test Complexes. The ligand−protein complexes used in this study are listed in Table 1. None of them contain atom types other than C, H, N, O, S, and P. Seventeen complexes were chosen as a training set to determine the optimal values of the descreening parameters in the HCT GB model. Fifteen complexes were used to test the prediction of the electrostatic binding energies using the optimized parameter set. The coordinates of the complexes were downloaded from the Protein Data Bank.[52] The AMBER all-atom force field parameters were used in the present study.[15] Water molecules were excluded in our calculations. AMBER all-atom charges were assigned to the proteins, and Gasteiger charges were assigned to the ligands, using the SYBYL software (Tripos, Inc.).

2.5. Optimization of the Descreening Parameters. We adopted the HCT GB model in which the descreening parameters are atom-type dependent.[1] Six atom types were used in the present work: carbon (C), hydrogen (H), nitrogen (N), oxygen (O), sulfur (S), and phosphorus (P). TINKER descreening parameters[53] were adopted for S (0.96) and P (0.86), due to the lack of sufficient statistics for parametrization. For optimization of the remaining four descreening parameters (S_C, S_H, S_N, S_O), the parameters were varied simultaneously and systematically. Specifically, each parameter was varied from 0.4 to 0.9 with an increment of 0.1, yielding a total of $6^4 = 1296$ combinations of $\{S_C, S_H, S_N, S_O\}$. We restrict S_C, S_H, S_N, and S_O below 0.9, because otherwise severe overlap between the rescaled atomic spheres would systematically overestimate the effective Born radii.[32] The results from the optimization of $\{S_C, S_H, S_N, S_O\}$ for solvation energies of small molecules[1,53] also show that the parameter range we chose is appropriate.

The following criteria were used for determination of the optimal descreening parameters for the HCT GB model. First, the effective Born radii calculated with the GB model should be comparable to those with the PB approach. Second, the GB results of G_{POL}, the electrostatic component of energies of binding, should agree well with the PB results. Finally, the GB calculations and PB calculations should correlate well on various decompositions of G_{POL}.

3. Results and Discussion

3.1. Deriving Optimal Descreening Parameters based on the Training Set.

3.1.1. Effective Born Radii. To evaluate how well the HCT GB model with different descreening parameters reproduces the effective Born radii obtained from the PB calculations, we used

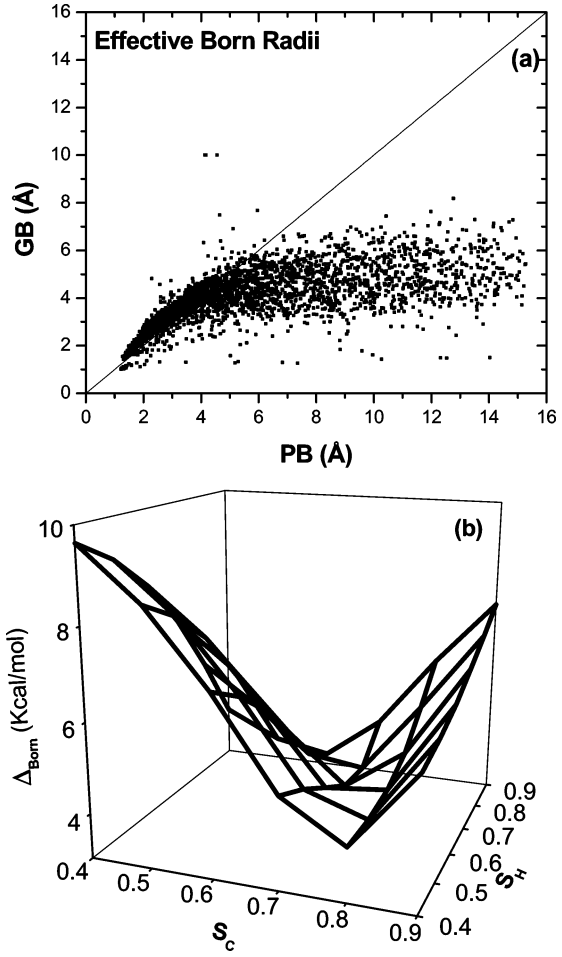

Figure 2. (a) Effective Born radii obtained from the HCT GB model with the descreening parameters $\{S_C, S_H, S_N, S_O\}$ set to {0.6, 0.8, 0.9, 0.8}, compared to those derived from the PB method. (b) Plot of the error function Δ_{Born} as a function of S_C and S_H when S_N and S_O were fixed to 0.9 and 0.8, respectively.

the following error function:

$$\Delta_{Born} = \sqrt{\frac{1}{N}\sum_i (G_{pol,i}^{GB} - G_{pol,i}^{PB})^2} \qquad (23)$$

where $G_{pol,i}^{GB}$ and $G_{pol,i}^{PB}$ represent the polarization energies of the system in which all of the atomic charges were set to zero except that the charge on atom i was set to unity, calculated with the GB and PB approaches, respectively. Note that this choice of the error function is based on $G_{pol,i}$ rather than the corresponding α_i, because minimization of the error function will bias toward atoms with smaller Born radii, which tend to make larger contributions to solvation energies and ligand binding energies.

Here, $G_{pol,i}^{GB}$ was calculated using eq 2, and $G_{pol,i}^{PB}$ was obtained from the corrected reaction field term in the DelPhi output for the system in which only the charge on the ith atom was turned on and set to unity. A threshold of 5 kcal/mol was set for Δ_{Born} to define a good reproduction of the effective Born radii. Only the complex of 3ptb-benz was used to optimize the descreening parameters against the Born radii, because our calculations on three other complexes (4dfr-mtx, 2ifb-PLM, and 6abp-ara) showed that the results were similar (data not shown).

For the GB calculations, among 1296 combinations of $\{S_C, S_H, S_N, S_O\}$, 7% gave good reproduction of the effective Born radii, namely, $\Delta_{Born} < 5$ kcal/mol. One of the parameter sets that fits the criterion of Δ_{Born} is {0.6, 0.8, 0.9, 0.8}. Figure 2a shows the effective Born radii calculated by the HCT GB model using this parameter set for the atoms in the 3ptb-benz complex, compared to the PB results. It can be seen from Figure 2a that the GB Born radii agree well with the PB Born radii for relatively exposed atoms ($\alpha < 5$ Å or $1/\alpha > 0.2$). The HCT GB method systematically underestimates the effective Born radii for deeply buried atoms. It is noticeable that eqs 6 and 7 occasionally yield negative Born radii, a phenomenon that was also observed in ref 47. Negative Born radii usually occur for the atoms that are heavily shielded by at least two intersected spheres nearby, because in these cases the overlapping volume between the intersected spheres is overcounted when calculating the contribution of the integral using eq 7. In the present work, $1/\alpha$ was set to 0.1 (equivalent to a Born radius of 10 Å) if the calculated value of $1/\alpha$ from eq 7 is less than 0.1. Because the energetic contribution is inversely proportional to the effective Born radii, the effect of setting the 10 Å cutoff would be limited.

A careful examination on the parameter space $\{S_C, S_H, S_N, S_O\}$ showed that, in certain regions, the error function Δ_{Born} was small when two descreening parameters were varied while the other two were fixed. One such example is given in Figure 2b. In the figure, the descreening parameters for nitrogen and oxygen, S_N and S_O, are fixed at 0.9 and 0.8, respectively. As the descreening parameters for carbon and hydrogen atoms vary, 15 of the 36 calculated Δ_{Born} values are less than 5 kcal/mol. Although the GB calculations using these 15 sets of descreening parameters resulted in effective Born radii values comparable to the PB results, not all of the parameter sets would give satisfactory results on the electrostatics of ligand binding (see below). The incapability of finding a unique combination of the descreening parameters suggests that the effective Born radii alone are insufficient to optimize the HCT GB parameters.

3.1.2. Electrostatic Solvation Energies. We next optimize the descreening parameters against the electrostatic solvation energies (i.e., the polarization energies) of the ligand and the receptor. The Pearson coefficient, R_P,[54] was used to measure the correlation between the GB results and PB results as follows:

$$R_P = \frac{\sum_i (x_i - \bar{x})(y_i - \bar{y})}{\sqrt{\sum_i (x_i - \bar{x})^2}\sqrt{\sum_i (y_i - \bar{y})^2}} \qquad (24)$$

where x and y represent the polarization energies calculated using the PB approach and those using the HCT GB model with different combinations of $\{S_C, S_H, S_N, S_O\}$. $\bar{x}$ and $\bar{y}$ denote the mean of x and y. The closer the coefficient to 1, the stronger the correlation between the two data sets. In the present work, a threshold of 0.95 was used for R_P to define a good correlation between the calculated polarization energies with the GB and PB methods. Seventeen ligand−protein complexes were used as a training set (see Table 1).

Among 1296 combinations of the descreening parameters in the HCT GB model, 44% gave R_P values greater than 0.95 for the polarization energies of the receptors and 64% of them did so for the polarization energies of the ligands. One of the $\{S_C, S_H, S_N, S_O\}$ parameter sets that satisfies the R_P criterion is {0.6, 0.8, 0.9, 0.8}. Figure 3a shows the comparison between the polarization energies calculated using this set of GB parameters and the energies obtained with DelPhi. The upper right points represent the 17 ligands extracted from the complexes in the training set, indicating an excellent agreement between the HCT GB model and the PB model for small molecules. The remaining

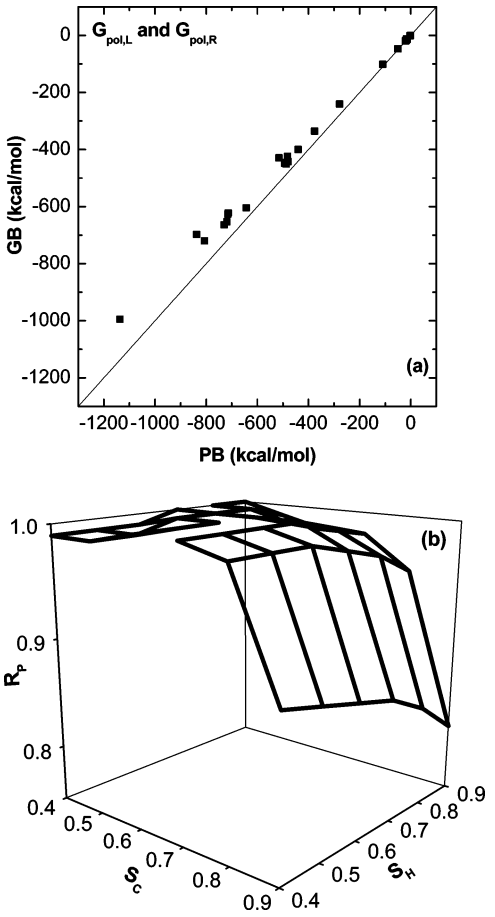

Figure 3. (a) Electrostatic component of the solvation energies ($G_{pol,R}$ for the receptors and $G_{pol,L}$ for the ligands) calculated by the HCT GB model with $\{S_C, S_H, S_N, S_O\}$ set to {0.6, 0.8, 0.9, 0.8} and compared with the PB results. The points in the upper right corner represent the results for the ligands, and the remaining points are for the receptors. (b) Plot of the correlation coefficient, R_P, as a function of S_C and S_H for $S_N = 0.9$ and $S_O = 0.8$.

points represent the 17 proteins. Overall, the two methods agree well on polarization energy calculations, except for an energy shift, which has also been observed in previous studies.[55]

It is worthwhile to understand why the polarization energies of the receptors can still be reasonably reproduced despite the rather dismal agreement of effective Born radii for deeply buried atoms. We found that, for the receptors, the self-energy term (i.e., the sum of all terms with $i = j$ on the right-hand side of eq 12) and the cross-energy term (i.e., the sum of all terms with $i \neq j$) have opposite signs and tend to compensate each other. Underestimation of the Born radii (α_i's) of the deeply buried atoms obviously decreases the magnitude of the self-energy term. In the meantime, the underestimation of α_i also decreases the function f_{GB}^R and leads to a reduction of the magnitude of the cross-energy term (data not shown). The errors in the self-energy term and the cross-energy term due to the underestimation of the Born radii of the deeply buried atoms thus tend to cancel, leading to good energy correlation in Figure 3a.

A thorough analysis of the R_P values by varying $\{S_C, S_H, S_N, S_O\}$ showed that the landscape of R_P was flat for certain combinations of the descreening parameters. One typical example is shown in Figure 3b. In this example, S_N and S_O were fixed to 0.9 and 0.8. The insensitivity of the calculated R_P for polarization energies on a wide range of S_C and S_H values indicates that the optimization procedure should go beyond polarization energies.

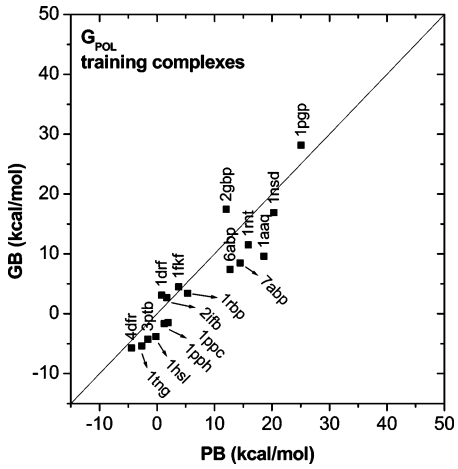

Figure 4. Electrostatic component of the energies of ligand binding, G_{POL}, for the training ligand−protein complexes calculated using the HCT GB model with $\{S_C, S_H, S_N, S_O\}$ set to {0.6, 0.8, 0.9, 0.8}, compared to the corresponding PB energies. The complexes are denoted by their PDB codes.

3.1.3. Electrostatic Binding Energies. To narrow down the appropriate parameter regime for $\{S_C, S_H, S_N, S_O\}$, the electrostatic component of ligand binding energies was calculated with the HCT GB model using the 1296 sets of the descreening parameters for 17 protein−ligand complexes. To compare with the PB results, the root-mean-square deviation, D_{POL}, was monitored:

$$D_{POL} = \sqrt{\frac{1}{N}\sum_i (G_{POL}^{GB} - G_{POL}^{PB})^2} \qquad (25)$$

where G_{POL}^{GB} and G_{POL}^{PB} are the calculated electrostatic component of the binding energy using the GB and the PB methods, respectively. The sum is over the 17 ligand−protein complexes in the training database. In the present study, a GB result is considered to be successful if the corresponding D_{POL} value is <6 kcal/mol.

Among 1296 combinations of $\{S_C, S_H, S_N, S_O\}$, 29% of them gave $D_{POL} < 6$ kcal/mol. Figure 4 shows the GB electrostatic binding energies using the descreening parameter set {0.6, 0.8, 0.9, 0.8} in comparison with the PB calculations. The R_P value is 0.92, and D_{POL} is 4.05 kcal/mol. It is dramatic that the PB results of the electrostatic component of ligand binding energies, G_{POL}, were reproduced well by the much simpler HCT GB model, especially considering the wide range of G_{POL} in this study (from ~ -5 to $\sim +25$ kcal/mol).

3.1.4. Partial Desolvation Energies of the Ligands and Proteins upon Binding. Next, different components of the electrostatic binding energies were analyzed. Specifically, the partial desolvation energies of the ligands and the proteins, $G_{L\ desolv}$ and $G_{R\ desolv}$, were calculated using eqs 16 and 17 with the GB method. For comparison, $G_{L\ desolv}$ and $G_{R\ desolv}$ were also calculated using eqs 19 and 21 with the PB method. The results show that the GB calculations correlate better with the PB calculations for $G_{L\ desolv}$ than $G_{R\ desolv}$. Therefore, in the present work, a threshold R_P value of 0.9 was considered as a satisfactory agreement between the two methods for the ligands, and 0.8 was set as the threshold of R_P for the proteins.

Among 1296 combinations of the descreening parameter sets in the HCT GB model, 72% of them result in good correlations with the PB calculations on $G_{L\ desolv}$ and 2% on $G_{R\ desolv}$. Figure 5 shows the comparison using {0.6, 0.8, 0.9, 0.8} for $\{S_C, S_H,$

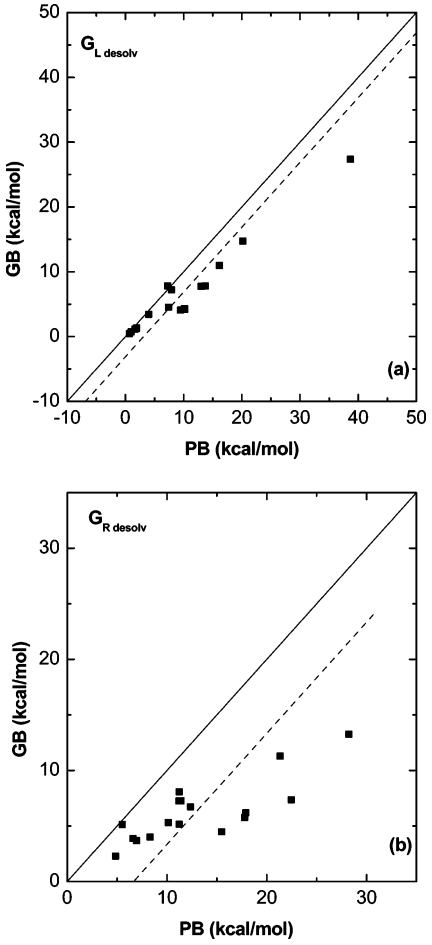

Figure 5. Partial desolvation energies of the ligand, $G_{L\ desolv}$ (panel a), and partial desolvation energies of the receptor, $G_{R\ desolv}$ (panel b), calculated using the HCT GB model with the descreening parameter set {0.6, 0.8, 0.9, 0.8}, compared to those calculated using the PB approach. The solid lines represent the perfect match. The dotted lines represent the best fit with a slope of 1; the shifts are −3.21 kcal/mol in panel a and −6.84 kcal/mol in panel b.

S_N, S_O}. In this case, the R_P values are 0.97 and 0.81 for $G_{L\ desolv}$ and $G_{R\ desolv}$, respectively.

3.1.5. Optimized Descreening Parameters. We have shown in previous sections that using one criterion alone fails to obtain a narrow range of optimized descreening parameters, with which the HCT GB results are comparable to PB calculations. Specifically, among 1296 combinations of {S_C, S_H, S_N, S_O} in the HCT GB model, 7% of them reproduce well the PB Born radii; 44 and 64% yield good correlation with the PB polarization energies for the proteins and the ligands, respectively; 29% give agreeable results on the electrostatic component of ligand binding energies; 2 and 72% correlate well with the PB approach on the partial desolvation energy of the protein and partial desolvation energy of the ligand, respectively. Combining all of these criteria allows us to identify 4 out of the 1296 parameter sets, with which the performance of the GB method is comparable to that of the PB method.

To better illustrate the parameter search results, we plotted a landscape of how the HCT GB model reproduces the PB results as a function of the descreening parameters in Figure 6. Here, to clearly show the variations in the landscape, we focused on the three most stringent criteria out of the aforementioned six criteria: the agreement between the HCT GB model and the PB approach on effective Born radii, the electrostatic component of binding energies, G_{POL}, and the partial desolvation energy

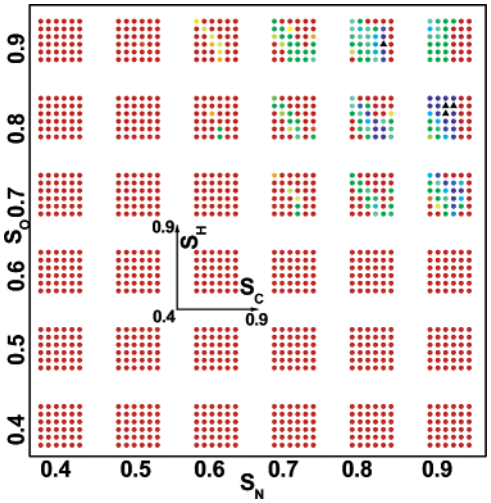

Figure 6. Landscape for the descreening parameter search. For each panel, the horizontal and vertical axes represent the descreening parameters for carbon, S_C, and hydrogen, S_H, respectively. Different rows and columns represent different descreening parameters for nitrogen, S_N, and oxygen, S_O, respectively. Every descreening parameter varies from 0.4 to 0.9, with an increment of 0.1. The color represents the average degree of acceptance of the descreening parameter set, with low degree in red and high degree in blue (see text for details). The parameter combinations that satisfy all criteria are shown as black triangles (see the two panels in the upper right corner).

of the receptor, $G_{R\ desolv}$. We introduced a variable, λ, the degree of acceptance, for each criterion that describes the extent of the agreement between GB and PB and varies between 0 and 1. λ is set to 1 when the criterion is satisfied and zero when the GB results are off from the PB results by a threshold. In the case of Born radii, λ_{Born} was 1 when $\Delta_{Born} \leq 5$ kcal/mol and zero when $\Delta_{Born} \geq 10$ kcal/mol (see eq 23). $\lambda_{G_{POL}}$ was 1 when $D_{POL} \leq 6$ kcal/mol and zero when $D_{POL} \geq 10$ kcal/mol (see eq 25). $\lambda_{G_{R\ desolv}}$ was set to 1 when the correlation coefficient, R_P, was higher than 0.8 and zero when $R_P \leq 0$. The λ values between 0 and 1 were linearly interpolated according to the degree of agreement between GB and PB. The geometric average of the three λ's as a function of the descreening parameters was then calculated and plotted in colors, with low values (i.e., poor agreement between GB and PB) in red and high values (i.e., good agreement) in blue. Figure 6 shows that most combinations of {S_C, S_H, S_N, S_O} for the HCT GB model poorly reproduce the PB results. There are four sets of {S_C, S_H, S_N, S_O} that satisfy all of the criteria, which were colored in black and plotted as triangles for better view.

The zoom-in landscape (data not shown) near the black triangles using a finer increment in descreening parameter values (0.02) shows that the appropriate parameter region, that is, the region in which the descreening parameter sets pass all six criteria, is well confined around the black triangles, an indication of the robustness of our aforementioned results. Moreover, the accuracy of reproducing the PB results with the parameter sets in this region was found to be comparable to that with the four parameter sets identified using the coarser parameter grid (with an increment of 0.1) and represented by the black triangles in Figure 6. Therefore, one of the black triangles, {0.6, 0.8, 0.9, 0.8}, was chosen and applied to study the electrostatics of ligand binding for 15 test complexes.

3.2. Electrostatic Energetics of the Test Ligand−Protein Complexes. A total of 15 ligand−protein complexes were selected to test the prediction of the electrostatic energetics of ligand binding with the HCT GB model using the optimized descreening parameter set, {0.6, 0.8, 0.9, 0.8} for {S_C, S_H, S_N,

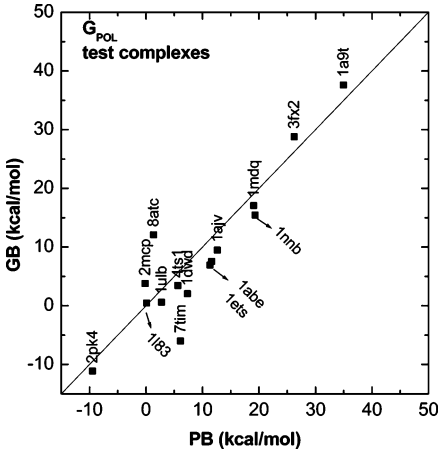

Figure 7. Electrostatic component of the energies of ligand binding, G_{POL}, for the ligand−protein complexes in the test set, calculated using the HCT GB model with $\{S_C, S_H, S_N, S_O\}$ set to {0.6, 0.8, 0.9, 0.8} and compared to the corresponding PB energies. The complexes are denoted by their PDB codes.

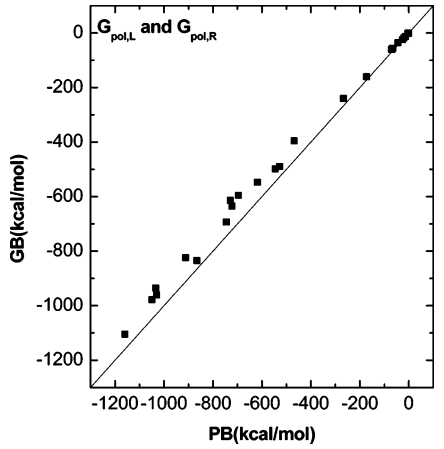

Figure 8. Electrostatic component of the solvation energies ($G_{pol,R}$ for the receptors and $G_{pol,L}$ for the ligands) for the ligands and proteins in the test set, calculated by the HCT GB model with the descreening parameter set {0.6, 0.8, 0.9, 0.8}, compared to those obtained from the PB approach. The points in the upper right corner represent the results for the ligands, and the remaining points are for the receptors.

$S_O\}$. The complexes are listed in Table 1. Figure 7 shows the calculated electrostatic component of the binding energy, using both GB and PB. The resulting R_P value is 0.91, and the root-mean-square deviation is 5.14 kcal/mol.

The electrostatic solvation energies (i.e., the polarization energies) of the ligand and the receptor were then calculated with the same set of descreening parameters. The results are shown in Figure 8. The HCT GB model agrees with the PB model very well, with a correlation coefficient of 0.99. The partial desolvation energy of the ligand and the partial desolvation energy of the protein were also calculated and plotted in Figure 9. Similar to the results for the training ligand−protein complexes, the HCT GB model performs well with the ligands ($R_P = 0.98$) and less well with the proteins ($R_P = 0.89$). Our detailed analysis shows that the underestimation of the effective Born radii for deeply buried atoms with the HCT method contributes to the less satisfactory correlation for the proteins than for the ligands on the comparison between the GB and PB partial desolvation energies. Specifically, upon ligand binding, the protein atoms located at the surface of the binding site become buried. Their effective Born radii before binding are quite accurately calculated with the HCT GB method, but their Born radii after binding are underestimated. The consequence

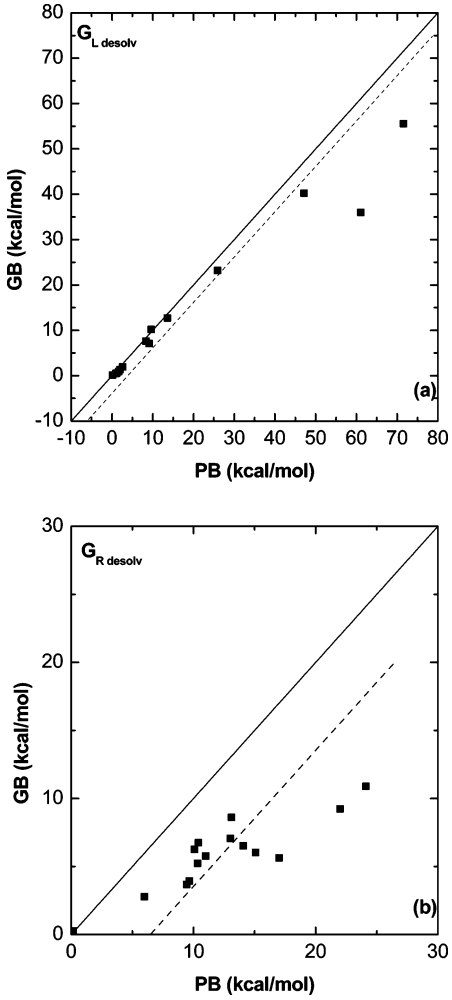

Figure 9. Partial desolvation energies of the ligand, $G_{L\ desolv}$ (panel a), and partial desolvation energies of the receptor, $G_{R\ desolv}$ (panel b), calculated using the HCT GB model with the descreening parameter set {0.6, 0.8, 0.9, 0.8}, compared to those calculated using the PB approach. The solid lines represent the perfect match. The dotted lines represent the best fit with a slope of 1; the shifts are −3.84 kcal/mol in panel a and −6.29 kcal/mol in panel b.

we found is the underestimation of the partial desolvation energies for the proteins. We further found that the cancellation of errors between the screened electrostatic energies and the partial desolvation energies of the proteins lead to a good agreement on the electrostatic component of the binding energies between the HCT GB method and the PB method.

To examine whether the cancellation of errors of the contributions of the deeply buried atoms is fortuitous, we did the following simple test in the GB scheme. Specifically, we exaggerated the underestimation of the Born radii of the surface protein atoms that become deeply buried upon ligand binding. Namely, we artificially decreased their postbinding Born radii by 1 Å each. Our calculated results show no significant changes in either the polarization energies of the complexes or the electrostatic component of the binding energies (data not shown). This suggests that, despite the rather dismal agreement of effective Born radii for deeply buried atoms, the cancellation of errors leads to reasonably good fits to PB calculated energies, likely due to the intrinsic nature of the GB scheme.

4. Conclusion and Discussion

The HCT GB model is a fast, widely used GB model that has been shown to be useful for ligand binding studies.[22] In the

present study, we have derived optimized descreening parameters for the HCT GB model in order to reproduce the PB results of effective Born radii, polarization energies (i.e., the electrostatic component of solvation energies), the electrostatic component of ligand binding energies, and its decompositions. Indeed, as pointed out by several groups,[39−41] we have found that polarization energies alone are insufficient for the comparison between the GB performance and PB performance. The narrow yet finite size of the appropriate parameter region obtained from our exhaustive parameter search suggests that there is no unique "best" parameter set, a reflection of the limitation of the HCT GB model. Although the AMBER force field and the HCT GB model were used in this work, the concept of parametrization against ligand binding can be applied easily to other force fields (including charge assignments[56]) combined with other GB models.

The set of descreening parameters $\{S_C, S_H, S_N, S_O\}$ chosen in this work is {0.6, 0.8, 0.9, 0.8}, which is different but not far from the widely used TINKER parameter set, {0.72, 0.85, 0.79, 0.85}.[53] The complexes selected for deriving and testing the optimized descreening parameters cover a wide variety of protein families and ligand types. Moreover, the electrostatic component of the binding energies, G_{POL}, calculated by the PB method spans a wide range, from −5 to +25 kcal/mol for the training set and from −10 to +35 kcal/mol for the test set. Our success in reproducing the PB results of G_{POL} with the HCT GB model is quite promising, considering the fact that the HCT GB model is simple and fast.

Several issues remain open for future studies. First, the effective Born radius of the isolated atom i (i.e., a_i in eq 5) could be irrelevant to its vdw radius.[32,38] The GB calculations with an alternative set of a_i showed improved agreement with the PB results.[38] Thus, the atom-type-dependent a_i could be treated as a set of fitted parameters to improve the ability of the GB method to reproduce the PB energies. Second, is the accuracy of Born radii a key issue for the GB models to reproduce the PB results on the electrostatics of ligand binding? Recently, Brooks and co-workers showed that an improved fit between GB and PB radii significantly increases the agreement of GB calculations with PB calculations on electrostatic solvation energies for protein structures.[45−47] Moreover, Onufriev et al.[57] performed GB calculations using PB-derived effective Born radii ("perfect" Born radii). They found that the PB cross-energy terms in solvation energies are better reproduced by the GB approach when perfect values of the Born radii are used. Thus, the importance of getting the effective Born radii right for studies on the electrostatics of ligand binding will be investigated. Third, several forms of the f_{GB} function have been proposed.[39,57] It is unclear what the best form of f_{GB} is for electrostatic studies on ligand binding. Onufriev et al.[57] reported that they were unable to find an expression of f_{GB} that is good for both the solvation energy term and its cross-energy component. They also argued that a modified f_{GB} function, compared with the standard f_{GB} expression, that gives closer agreement with the PB model when the perfect Born radii are used may not be optimal with less-than-perfect Born radii. These observations imply some inherent problem with the simple GB models. Our ongoing efforts seek to find an alternative approach for the GB models. After all, the calculated electrostatic energies and their components are the quantities of real interest. The Born radii and f_{GB} are simply functional forms useful for approximating solvation electrostatics and could be replaced by other simple approximations.

Acknowledgment. Support from Tripos, Inc. (St. Louis, MO), is gratefully acknowledged. This work is supported by the Research Board Award of the University of Missouri, AHA grant 0265293Z (Heartland Affiliate) and NIH grant DK61529.

References and Notes

(1) Hawkins, G. D.; Cramer, C. J.; Truhlar, D. G. *Chem. Phys. Lett.* **1995**, *246*, 122−9.
(2) Leach, A. R. *Molecular Modeling: Principles and Applications*; Longman: Singapore, 1996.
(3) Wang, W.; Donini, O., Reyes, C. M.; Kollman, P. A. *Annu. Rev. Biophys. Biomol. Struct.* **2001**, *30*, 211−43.
(4) Lamb, M. L.; Jorgensen, W. L. *Curr. Opin. Chem. Biol.* **1997**, *1*, 449−57.
(5) Cramer, C. J.; Truhlar, D. G. *Chem. Rev.* **1999**, *99*, 2161−200.
(6) Roux, B.; Simonson, T. *Biophys. Chem.* **1999**, *78*, 1−20.
(7) Simonson, T. *Curr. Opin. Struct. Biol.* **2001**, *11*, 243−52.
(8) Gilson, M. K.; Sharp, K. A.; Honig, B. *J. Comput. Chem.* **1987**, *9*, 327−35.
(9) Rocchia, W.; Sridharan, S.; Nicholls, A.; Alexov, E.; Chiabrera, A.; Honig, B. *J. Comput. Chem.* **2002**, *23*, 128−137.
(10) Grant, J. A.; Pickup, B. T.; Nicholls, A. *J. Comput. Chem.* **2001**, *22*, 608−40.
(11) Baker, N. A.; Sept, D.; Joseph, S.; Holst, M. J.; McCammon, J. A. *Proc. Natl. Acad. Sci. U.S.A.* **2001**, *98*, 10037−41.
(12) Still, W. C.; Tempczyk, A.; Hawley, R. C.; Hendrickson, T. *J. Am. Chem. Soc.* **1990**, *112*, 6127−9.
(13) Bashford, D.; Case, D. A. *Annu. Rev. Phys. Chem.* **2000**, *51*, 129−52.
(14) Brooks, B. R.; Bruccoleri, B. D.; Olafson, B. D.; States, D. J.; Swaminathan, S.; Karplus, M. *J. Comput. Chem.* **1983**, *4*, 187−217.
(15) Cornell, W. D.; Cieplak, P.; Bayly, C. I.; Gould, I. R.; Merz, K.; Ferguson, D. M.; Spellmeyer, D. C.; Fox, T.; Caldwell, J. W.; Kollman, P. A. *J. Am. Chem. Soc.* **1995**, *117*, 5179−97.
(16) Banks, J. L.; Beard, H. S.; Cao, Y.; Cho, A. E.; Damm, W.; Farid, R.; Felts, A. K.; Halgren, T. A.; Mainz, D. T.; Maple, J. R.; Murphy, R.; Philipp, D. M.; Repasky, M. P.; Zhang, L. Y.; Berne, B. J.; Friesner, R. A.; Gallicchio, E.; Levy, R. M. *J. Comput. Chem.* **2005**, *26*, 1752−80.
(17) Christen, M.; Hunenberger, P. H.; Bakowies, D.; Baron, R.; Burgi, R.; Geerke, D. P.; Heinz, T. N.; Kastenholz, M. A.; Krautler, V.; Oostenbrink, C.; Peter, C.; Trzesniak, D.; van Gunsteren, W. F. *J. Comput. Chem.* **2005**, *26*, 1719−51.
(18) Ren, P.; Ponder, J. W. *J. Phys. Chem. B* **2003**, *107*, 5933−47.
(19) Jorgensen, W. L.; Tirado-Rives, J. *J. Comput. Chem.* **2005**, *26*, 1689−700.
(20) Zou, X.; Sun, Y.; Kuntz, I. D. *J. Am. Chem. Soc.* **1999**, *121*, 8033−43.
(21) Ewing, T. J.; Makino, S.; Skillman, A. G.; Kuntz, I. D. *J. Comput.-Aided Mol. Des.* **2001**, *15*, 411−28.
(22) Liu, H. Y.; Kuntz, I. D.; Zou, X. *J. Phys. Chem. B* **2004**, *108*, 5453−62.
(23) http://dock.compbio.ucsf.edu/DOCK_5/index.htm.
(24) Majeux, N.; Scarsi, M.; Apostolakis, J.; Ehrhardt, C.; Caflisch, A. *Proteins* **1999**, *37*, 88−105.
(25) Cecchini, M.; Kolb, P.; Majeux, N.; Caflisch, A. *J. Comput. Chem.* **2004**, *25*, 412−22.
(26) Huang, D.; Luthi, U.; Kolb, P.; Edler, K.; Cecchini, M.; Audetat, S.; Barberis, A.; Caflisch, A. *J. Med. Chem.* **2005**, *48*, 5108−11.
(27) Cho, A. E.; Wendel, J. A.; Vaidehi, N.; Kekenes-Huskey, P. M.; Floriano, W. B.; Maiti, P. K.; Goddard, W. A., III. *J. Comput. Chem.* **2005**, *26*, 48−71.
(28) Ghosh, A.; Rapp, C. S.; Friesner, R. A. *J. Phys. Chem. B* **1998**, *102*, 10983−90.
(29) Jacobson, M. P.; Pincus, D. L.; Rapp, C. S.; Day, T. J.; Honig, B.; Shaw, D. E.; Friesner, R. A. *Proteins* **2004**, *55*, 351−67.
(30) Lorber, D. M.; Shoichet, B. K. *Protein Sci.* **1998**, *7*, 938−50.
(31) Halgren, T. A.; Murphy, R. B.; Friesner, R. A.; Beard, H. S.; Frye, L. L.; Pollard, W. T.; Banks, J. L. *J. Med. Chem.* **2004**, *47*, 1750−9.
(32) Hawkins, G. D.; Cramer, C. J.; Truhlar, D. G. *J. Phys. Chem.* **1996**, *100*, 19824−39.
(33) Jayaram, B.; Sprous, D.; Beveridge, D. L. *J. Phys. Chem. B* **1998**, *102*, 9571−6.
(34) Srinivasan, J.; Trevathan, M. W.; Beroza, P.; Case, D. A. *Theor. Chem. Acc.* **1999**, *101*, 426−34.
(35) Dominy, B. N.; Brooks, C. L., III. *J. Phys. Chem. B* **1999**, *103*, 3765−73.
(36) Onufriev, A.; Bashford, D.; Case, D. A. *J. Phys. Chem. B* **2000**, *104*, 3712−20.
(37) Tsui, V.; Case, D. A. *J. Am. Chem. Soc.* **2000**, *122*, 2489−98.
(38) Zhang, W.; Hou, T.; Qiao, X.; Xu, X. *J. Phys. Chem. B* **2003**, *107*, 9071−8.

(39) Jayaram, B.; Liu, Y.; Beveridge, D. L. *J. Chem. Phys.* **1998**, *109*, 1465−71.
(40) Scarsi, M.; Caflisch, A. *J. Comput. Chem.* **1999**, *20*, 1533−6.
(41) Scarsi, M.; Apostolakis, J.; Caflisch, A. *J. Phys. Chem. A* **1997**, *101*, 8098−8106.
(42) Rankin, K. N.; Sulea, T.; Purisima, E. O. *J. Comput. Chem.* **2003**, *24*, 954−62.
(43) Qiu, D.; Shenkin, P. S.; Hollinger, F. P.; Still, W. C. *J. Phys. Chem. A* **1997**, *101*, 3005−14.
(44) Gallicchio, E.; Levy, R. M. *J. Comput. Chem.* **2004**, *25*, 479−99.
(45) Lee, M. S.; Salsbury, F. R., Jr.; Brooks, C. L., III. *J. Chem. Phys.* **2002**, *116*, 10606−14.
(46) Lee, M. S.; Salsbury, F. R., Jr.; Brooks, C. L., III. *J. Comput. Chem.* **2003**, *24*, 1348−56.
(47) Feig, M.; Onufriev, A.; Lee, M. S.; Im, M.; Case, D. A.; Brooks, C. L., III. *J. Comput. Chem.* **2004**, *25*, 265−84.
(48) Zhu J.; Alexov, E.; Honig, B. *J. Phys. Chem. B* **2005**, *109*, 3008−22.
(49) Born, M. *Z. Phys.* **1920**, *1*, 45−8.
(50) Schaefer, M.; Karplus, M. *J. Phys. Chem.* **1996**, *100*, 1578−99.
(51) Gilson, M. K.; Honig, B. *Proteins* **1988**, *4*, 7−18.
(52) Berman, H. M.; Westbrook, J.; Feng, Z.; Gilliland, G.; Bhat, T. N.; Weissig, H.; Shindyalov, I. N.; Bourne, P. E. *Nucleic Acids Res.* **2000**, *28*, 235−42.
(53) Ponder, J. W. http://dasher.wustl.edu/tinker.
(54) Press: W. H.; Teukolsky, S. A.; Vetterling, W. T.; Flannery, B. P. *Numberical recipes in FORTRAN*; Cambridge University Press: New York, 1994.
(55) Edinger, S. R.; Cortis, C.; Shenkin, P. S.; Fiesner, R. A. *J. Phys. Chem. B* **1997**, *101*, 1190−7.
(56) Wei, B. Q. Q.; Baase, W. A.; Weaver, L. H.; Matthews, B. W.; Shoichet, B. K. *J. Mol. Biol.* **2002**, *322*, 339−55.
(57) Onufriev, A.; Case, D. A.; Bashford, D. *J. Comput. Chem.* **2002**, *23*, 1297−304.